Nucleic Acids Research, 2024, 1–12
https://doi.org/10.1093/nar/gkae249
Genome integrity, repair and replication

Ordered and disordered regions of the Origin Recognition Complex direct differential *in vivo* binding at distinct motif sequences

Michal Chappleboim[1], Segev Naveh-Tassa[2], Miri Carmi[1], Yaakov Levy[2] and Naama Barkai[1,*]

[1]Department of Molecular Genetics, Weizmann Institute of Science, Rehovot, Israel
[2]Department of Chemical and structural Biology, Weizmann Institute of Science, Rehovot, Israel
[*]To whom correspondence should be addressed. Tel: +972 8 934 3971; Email: naama.barkai@weizmann.ac.il

Abstract

The Origin Recognition Complex (ORC) seeds replication-fork formation by binding to DNA replication origins, which in budding yeast contain a 17bp DNA motif. High resolution structure of the ORC-DNA complex revealed two base-interacting elements: a disordered basic patch (Orc1-BP4) and an insertion helix (Orc4-IH). To define the ORC elements guiding its DNA binding *in vivo,* we mapped genomic locations of 38 designed ORC mutants, revealing that different ORC elements guide binding at different sites. At silencing-associated sites lacking the motif, ORC binding and activity were fully explained by a BAH domain. Within replication origins, we reveal two dominating motif variants showing differential binding modes and symmetry: a non-repetitive motif whose binding requires Orc1-BP4 and Orc4-IH, and a repetitive one where another basic patch, Orc1-BP3, can replace Orc4-IH. Disordered basic patches are therefore key for ORC-motif binding *in vivo,* and we discuss how these conserved, minor-groove interacting elements can guide specific ORC-DNA recognition.

Graphical abstract

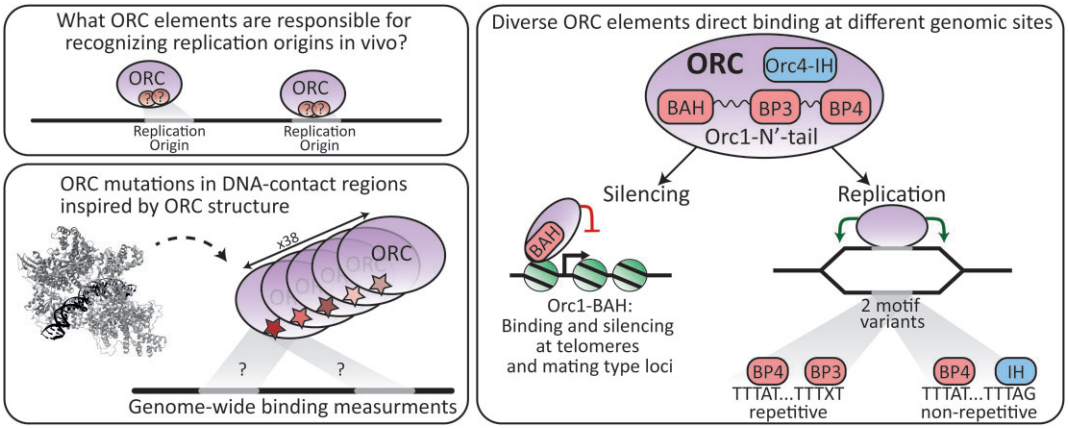

Introduction

In eukaryotes, DNA replication is initiated by firing numerous replication origins across the genome, ranging from hundreds in yeast to tens of thousands in mammals (1–6). The Origin Recognition Complex (ORC) binds replication origins and recruits the replication machinery. In budding yeast, ORC identifies the replication origins, referred to as ARS (Autonomous Replicating Sequences), through a consensus 17-bp T-rich motif (7–16) called EACS (Extended ARS Consensus Sequence), while in higher eukaryotes, ORC binding sites lack an apparent motif but are still enriched with T-stretches (17–21).

A high-resolution cryo-EM structure of the *Saccharomyces cerevisiae* ORC bound to DNA is available (22), showing that all six ORC subunits are engaged in backbone interactions. Only two elements, however, formed specific base contacts: an insertion helix within Orc4 (Orc4-IH) and a basic patch (Orc1-BP4) within Orc1. These ORC-DNA specific contacts, in turn, were limited to five of the seventeen base-pair EACS (22). Orc4-IH is unique to budding yeast and its close phylogenetic relatives (23,24), whereas basic patches, defined as >5 basic residues within a 10–14 AA stretch, are conserved features of Orc1 N-terminus across eukaryotes (22), although with varying sequences and locations.

Inferring principles of *in vivo* binding from structural data is challenging. First, ORC binds to hundreds of genomic sites with different motif variants, while the structure describes

Received: January 10, 2024. **Revised:** March 16, 2024. **Editorial Decision:** March 23, 2024. **Accepted:** April 9, 2024

only one bound sequence. Second, *in vitro* analysis often relies on truncated proteins that are easier to express and purify. In the ORC-DNA structure, for example, Orc1 lacks most of its disordered N-terminus (Figure 1A) (22). Third, chromatin and other accessory proteins that could influence *in vivo* binding are missing from the structure. Finally, cryo-EM structures capture only conformations of sufficient stability, while genomic preferences could depend on contacts that are required transiently for reaching the stable configuration.

Here, we defined ORC elements required for its *in vivo* DNA binding by mapping the genomic binding of 38 designed ORC mutants. We describe three classes of ORC binding sites that depend on distinct ORC elements. The first class comprises EACS-lacking sites, usually in silenced gene promoters, where ORC is involved in gene silencing (25), and this binding is fully explained by Orc1 Bromo-Adjacent Homology (BAH) domain. The other two classes include strongly bound replication origins, which we are further divided based on two dominating motif variants: a repetitive motif consisting of a leading sub-motif with a TTTAT stretch and a trailing sub-motif with a TTTxT stretch, and a non-repetitive motif where the trailing sub-motif is replaced by TTTAG. Orc1-BP4 is necessary for binding at both motifs, while Orc4-IH is required for the non-repetitive one, but can be replaced by another basic patch, Orc1-BP3, at the repetitive variant. We discuss the possible implications of our results for the mechanism of ORC-DNA binding *in vivo* and its conservation across evolution.

Materials and methods

Yeast strains

All strains used in this study are derived from the wild-type *Saccharomyces cerevisiae* strain, BY4741 (genotype: MATa his3D1 leu2D0 met15D0 ura3D0). Specific genotypes of all strains used in this study are available in Supplementary Table S1.

Genetic manipulations

Yeast strains were freshly thawed before experiments from a frozen stock, plated on YPD plates, and incubated in 30°C. Single colonies were picked and grown in liquid YPD medium at 30°C with constant shaking. DNA editing was generated with the CRISP-Cas9 system (26). To this end, a PCR-amplified repair template or a synthetic oligo harboring the desired modification flaked by 50-bp homology was co-transformed alongside the bRA89 plasmid bearing Cas9 and the locus-specific 20-bp guide-RNA (from James Haber, Addgene plasmid no. 100950). Ligation of the locus-specific guide-RNA into the bRA89 plasmid was performed for each guide-RNA as previously described (27). After validation of yeast positive colonies, the bRA89 plasmid was lost by growth in YPD, followed by the selection of colonies that lost the bRA89 Hygromycin resistance.

All transformations were performed using the standard LiAc/SS DNA/PEG method (28). Briefly, a single colony was inoculated in fresh liquid YPD, grown to saturation overnight, diluted into fresh 5 ml YPD, and grown to OD_{600} of 0.5. The cells were then washed with DDW and then with LiAc 100 mM, and resuspended in transformation mix (33% PEG-3350, 100 mM LiAc, single stranded salmon sperm DNA, plasmid and the DNA repair). The cells were incubated at 30°C for 30 minutes followed by a 30-minute heat shock at 42°C. The cells were then plated on YPD plates and grown overnight in 30°C for recovery.

For strains containing an additional copy of the wild-type Orc1, a synthetic DNA block coding the wild-type ORC1 protein with numerous synonymous mutations (sequence in Supplementary Document S1) was inserted into the genome. This was done along with the original Orc1 promoter and into the Bar1 locus, creating a bar1 deletion. Additional genetic modifications were carried out by specifically targeting only the endogenous Orc1, using guide-RNAs that did not match the synonymous sequence of the synthetic Orc1.

Chec-seq experiments

The experiments were performed as described previously (29), with some modifications. Yeast strains were freshly thawed before experiments from frozen stocks, plated on YPD plates, and incubated at 30°C. Single colonies were picked and grown overnight at 30°C with constant shaking in liquid YPD medium to stationary phase. Then, the cultures were diluted into 15 ml fresh YPD media and grown overnight at 30°C to reach log-phase in the following morning. Cultures were pelleted at 1500 g for 2 min and resuspended in 0.5 ml buffer A (15 mM Tris pH 7.5, 80 mM KCl, 0.1 mM EGTA, 0.2 mM spermine, 0.5 mM spermidine, 13 cOmplete EDTA-free protease inhibitors (one tablet per 50 ml buffer), 1 mM PMSF) and then transferred to 2.2 ml 96-well plates (LifeGene). Cells were washed twice in 1 ml Buffer A. Next, the cells were resuspended in 150 ml Buffer A containing 0.1% digitonin, transferred to an Eppendorf 96-well plate (Eppendorf 951020401), and incubated at 30°C for 5 min for permeabilization. Next, $CaCl_2$ was added to a final concentration of 2 mM to activate the MNase and incubated for exactly 30 seconds. The MNase cleavage was stopped by adding an equal volume of stop buffer (400 mM NaCl, 20 mM EDTA, 4 mM EGTA, and 1% SDS) to the cell suspension. After this, the cells were treated with Proteinase K (0.5 mg/ml) at 55°C for 30 minutes. An equal volume of phenol-chloroform pH 8 (Sigma-Aldrich) was added, vigorously vortexed, and centrifuged at 17 000g for 10 min to extract DNA. After phenol-chloroform extraction of nucleic acids, the DNA was precipitated with 2.5 volumes of cold 96% EtOH, 45 mg Glycoblue (Thermo Fisher), and 20 mM sodium acetate at –80°C for >1 h. DNA was centrifuged (17 000g, 4°C for 10 min), the supernatant removed, and the DNA pellet washed with 70% EtOH at room temperature. DNA pellets were dried and resuspended in 30 ml RNase A solution (0.33 mg/ml RNase A in Tris–EDTA [TE] buffer [10 mM Tris and 1 mM EDTA]) and treated at 37°C for 20 min. To enrich for small DNA fragments, the samples went through reverse SPRI cleanup by adding 0.83 SPRI beads (Ampure XP). The supernatant was collected, and the remaining small DNA fragments were purified by adding an additional 13 SPRI beads and 5.43 isopropanol, and incubating for 5 min at RT. Beads were washed twice with 85% EtOH, and small fragments were eluted in 30 ml of 0.13 TE buffer.

Next generation sequencing library preparation

Library preparation was performed as described by Skene and Henikoff (30) with slight modifications. DNA fragments after RNase treatment and reverse SPRI cleanup served as an input to end-repair and an A-tailing (ERA) reaction. For each sample, 20 ml ERA reaction (13 T4 DNA ligase buffer [NEB], 0.5

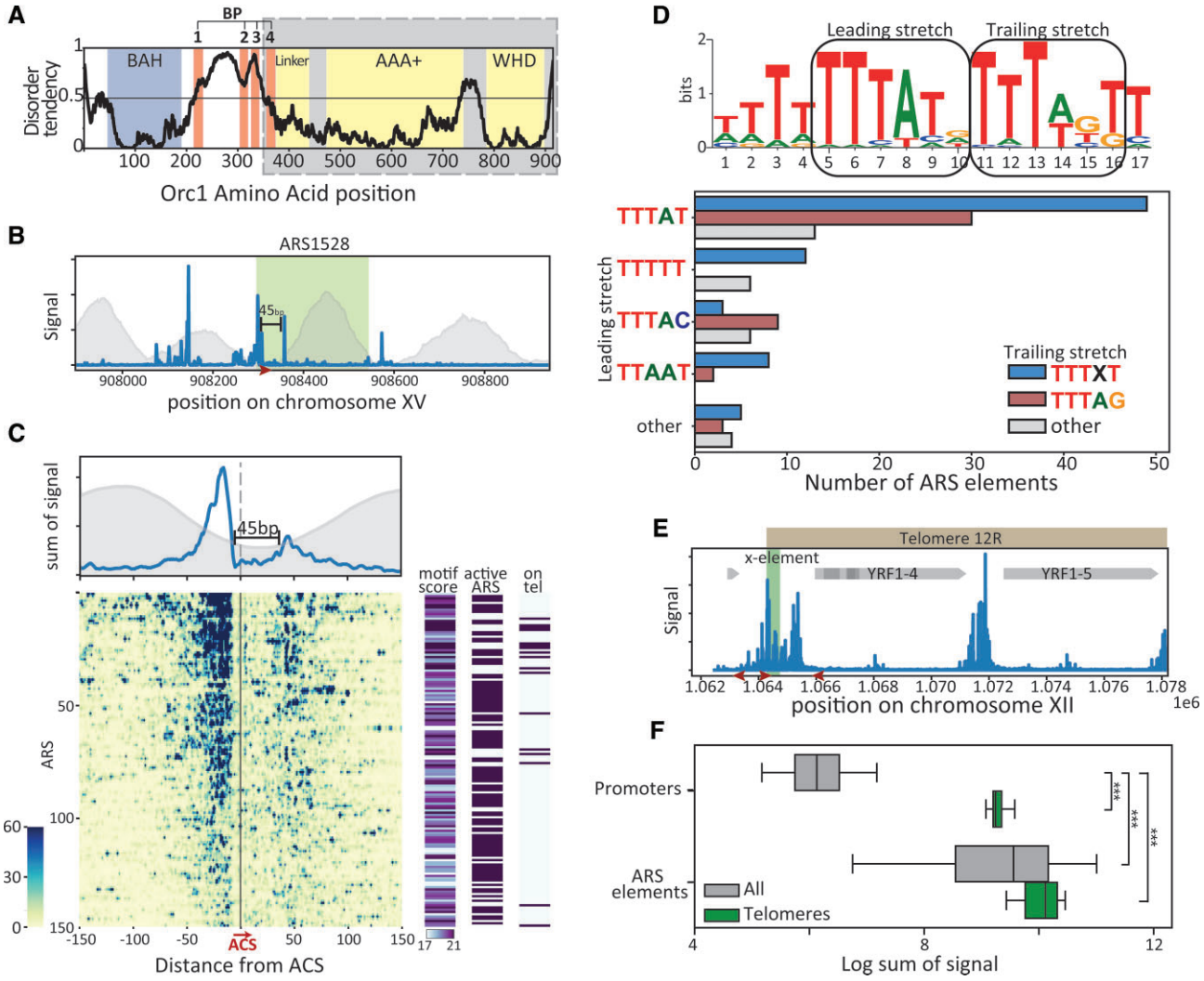

Figure 1. Genome-wide mapping of ORC binding locations reveals two prevailing motif sequences that dominate top-bound origins. (**A**) *Predicted disorder tendency of S.cerevisiae Orc1*: The black line indicates the predicted disorder tendency along the Orc1 protein sequence, as calculated by IUPred (60,61). Values above 0.5 are considered disordered. Colored regions indicate characterized domains (BAH: bromo-adjacent homology, BP: 4 basic patches, AAA+: ATPase associated activity, WHD: winged helix domain). The cryo-EM structure (22) was solved using a truncated Orc1, containing the 355–914 AA (Gray). (**B**) *Orc1 binding at a representative origin* (ARS1528): Shown is the normalized binding signal of Orc1 mapped to the indicated genomic segment containing a defined origin (see Methods for read alignment). The red arrow indicates the position and orientation of the ARS Consensus Sequence (ACS). Nucleosome occupancy is indicated in gray (data from Chapal *et al.* (62)). (**C**) *Orc1 binding across replication origins (ARSs):* origins and their surrounding 300 bp segments were aligned and oriented by the ACS. Shown are the average signal (top) and the mapped reads (bottom) of the 150 top-bound origins, ordered by the total Orc1 reads. The right columns depict the motif score and ARS replication activity (by Yabuki *et al.* (63)) of each sequence, and whether it localizes to a telomere. (**D**). *Top-bound origins contain two dominating motif variants:* the ORC motif by YeTFaSCo (35) (top) and the count of different motif variants present (bottom) among the 150 top-bound origins. (**E**). *Orc1 binding at the 12R telomere:* Shown is the Orc1 binding signal along the indicated region. The x-element is indicated by a green area. Red arrows indicate the position and orientation of ORC binding motifs, and gray arrows indicate open reading frames (ORFs). Note the strong binding signal at the motif bordering the x-element, and at the promoters of the silenced YRF1-4 and YRF1-5 genes. (**F**). *Orc1 binds gene promoters on telomeres:* Shown are the distributions of Orc1 binding at origins and promoters found away or near telomeres, as indicated. (Distributions shown as box-plots, see methods).

mM dNTPs, 0.25 mM ATP, 2.75% PEG 4000, 6U T4 PNK [NEB], 0.5 U T4 DNA Polymerase [Thermo Scientific] and 0.5 U Taq DNA polymerase [Bioline]) was prepared and incubated for 20 min at 12°C, 15 min at 37°C and 45 min at 58°C in a thermocycler. After ERA reaction, reverse SPRI cleanup was performed by adding 0.53 (10 ml) SPRI beads (Ampure XP). The supernatant was collected, and the remaining small DNA fragments were purified with additional 1.33 (26 ml) SPRI beads and 5.43 (108 ml) isopropanol. After washing with 85% EtOH, small fragments were eluted in 17 ml of 0.13 TE buffer; 16.4 ml elution was taken into 40 ml ligation reaction (13 Quick ligase buffer [NEB], 4000 U Quick ligase [NEB] and 6.4 nM Y-shaped barcode adaptors with T-overhang (31) and incubated for 15 min at 20°C in a thermocycler. After incubation, the ligation reaction was cleaned by performing a double SPRI cleanup: first, a regular 1.23 (48 ml) SPRI cleanup was performed and eluted in 30 ml 0.13 TE buffer. Then and instead of separating the beads, an additional SPRI cleanup was performed by adding 1.33 (39 ml) HXN buffer (2.5 M NaCl, 20% PEG 8000) and final elution in 24 ml 0.13 TE buffer; 23 ml elution were taken into 50 ml enrichment PCR reaction (13 Kappa HIFI [Roche], 0.32 mM barcoded Fwd primer and 0.32 mM barcoded Rev primer (31), and incubated for 45 s in 98°C, 16 cycles of 15 s in 98°C

and 15 s in 60°C, and a final elongation step of 1 min at 72°C in a thermocycler. The final libraries were cleaned by a regular 1.13 (55 ml) SPRI cleanup and eluted in 15 ml 0.13 TE buffer. Library concentration and size distribution were quantified by Qubit (Thermo Scientific) and TapeStation (Agilent), respectively. For multiplexed next-generation sequencing (NGS), all barcoded libraries were pooled in equal amounts, the final pool diluted to 2 nM and sequenced on NovaSeq 6000 (Illumina).

Process and analysis of ChEC-seq data

Raw paired end reads from ChEC-seq libraries were demultiplexed using bcl2fastq (Illumina), and adaptor dimers and short reads were filtered out using cutadapt (32) with parameters: '-O 10 –pair-filter = any -max-n 0.8 -action = mask'. Filtered reads were subsequently aligned to the *S. cerevisiae* genome R64-1-1 using Bowtie 2 (33) with the options '-end-to-end -trim-to 30 -very-sensitive'. The genome coverage was calculated using only the end positions of the fully aligned read pairs which correspond to the actual MNase cutting sites. Each sample was normalized to one million reads to control for sequencing depth variations. ARS, ORF and telomere annotations were taken from the SGD project (34). For each ARS element, the sub-sequence within the defined ARS borders, with the highest motif score was selected, and the signal within a window of 75 pb upstream and downstream to it was calculated. Motif scores were calculated using the PWM matrix from YeTFaSCo (35). To determine the presence of a motif within a sequence, scores were calculated for each subsequence within the entire sequence. A motif was deemed present if the score exceeded that of a sequence comprising exclusively T nucleotides.

Automated growth rate experiments

Cells were grown to stationary phase in YPD media in 96-well plates under constant shaking and at 30°C. Then, cells were diluted with fresh YPD media to OD_{600} 0.1. Plates were inserted into an automated handling robot (EVOware, Tecan Inc.) in which cells were grown in an incubator under constant shaking and 30°C. The robot was programed to take the plates out of the incubator every 30 min, vortex the plates, and measure the OD (using infinite200 reader, Tecan Inc.). Experiments lasted for approximately 40 h. OD measurements were parsed and processed from the reader output files. Growth rates were calculated as the maximal slope of the OD measurements (versus time). For each strain the mean value over six repeats was calculated.

Alpha factor imaging

Yeast strains (with bar1 deletion) were freshly thawed before experiments from frozen stocks, plated on YPD plates, and incubated at 30°C. Single colonies were picked and grown overnight at 30°C and constant shaking in liquid YPD medium to stationary phase. Then, the cultures were diluted into fresh YPD media and grown overnight at 30°C to reach log-phase in the following morning (OD_{600} 0.2). α-factor was added to the cells to a final concentration of 5 ng/ml α-factor (GenScript RP01002) for 3 h. Cells were attached to 18-well µ-Slide (Ibidi) pre-treated with Concanavalin A (ConA): 75 µl of 0.2 mg/µl ConA (Sigma-Aldrich) was added to each well and incubated at room temperature for 15 min. Subsequently, liquid was removed, and wells were air dried for 30 min. Then, 100 µl of the cell samples were added to the wells and incubated for 15 min, followed by a gentle wash with fresh media (with α-factor) to remove unattached cells. Imaging was done using a DMi8 microscope from Leica, integrated into a Dragonfly 505 from AndOr. AndOr's Fusion software was used for data acquisition.

Process and analysis of imaging data

Cells were segmented using a freely available yeast segmentation software (36). Cell classification was performed semi-manually by presenting a single random cell each time from all images, without disclosing the specific strain, for the user to label.

All-atom molecular dynamics simulations

To elucidate the structural dynamics of the ORC-DNA complex, we used all-atom molecular dynamics simulations via GROMACS (37). The simulations were initiated using the conformation derived from the resolved structure of the ORC-DNA complex (PDB ID 5ZR1). This included integrating the Orc1-BP4 region (Orc1 aa 356–373) and a 20-nucleotide segment from each DNA strand, which encompassed the ARS sequence based on PDB 5ZR1 (TGGTTTTTATATGTTTTGTT), serving as the control (WT).

In addition to the WT ORC-DNA complex, we simulated various mutants. Mutations were incorporated into the ORC protein based on experimentally examined mutants. Additionally, we selectively chose nucleotide alterations for DNA to evaluate their impact on peptide binding. To ensure the reliability of our results, we conducted three independent simulation runs for each mutation type. Mutations were manually introduced using PyMol, and the simulations spanned 1 µs, aiming to comprehensively capture the dynamics of molecular interactions. To more accurately mimic the movement of DNA and reflect the constraints imposed by the length and size of the DNA-protein complex, we implemented movement constraints. This involved fixing the positions of the DNA ends to stabilize their locations while still allowing the strands to exhibit dynamic behavior within these boundaries.

The simulation environment was set up within a solvated box under periodic boundary conditions, maintained at 300K. We used pre-equilibrated TIP3P water molecules and employed the Amber99 force field. After minimizing the system with the steepest descent algorithm, we conducted equilibration phases under NVT and NPT ensembles (each lasting 100 ps), followed by production runs at a constant pressure of 1 atm for 1 µs. This resulted in a total simulation time of 63 µs across all repetitions. Each variant was analyzed by calculating its RMSD (Root Mean Square Deviation) values relative to the initial structure model based on the EM structure. The mean RMSD and its standard deviation were used to assess changes in conformational stability caused by different mutations, comparing these changes directly to the baseline stability of the WT ORC-DNA complex.

Box plots

Boxes capture 25 to 75 percentiles; median is shown inside the boxes and the whiskers capture 10 to 90 percentiles. P-values are shown in asterisks: * < 0.05, ** < 0.01, *** < 0.001.

Results

Replication origins contain two dominating ORC-bound motif sequences that differ in symmetry

To map the genomic binding locations of ORC, we used the spatially resolved method ChEC-seq (29), where individual fusion of three ORC subunits (Orc1,2,4) to MNase enabled to trigger cleavage of DNA-bound sites through a short calcium pulse. The short DNA fragments, released by multiple nuclease cleavages adjacent to the MNase-fused protein, reveal the footprint of the protein with a single base-pair resolution. All three ORC subunits localized to the same genomic sites (Supplementary Figure S1A), which were consistent with previous ChIP-seq data (38), as expected (Supplementary Figure S1B), and exhibited a similar footprint (Supplementary Figure S1C). We selected Orc1 as our reporter for subsequent analysis.

Orc1 was bound to its known motif within a large fraction of replication origins. Our high- resolution data captured its footprint, as described *in vitro* (45–50 base pairs (39–43); Figure 1B, C) and further enabled the refinement of the EACS. This highlighted two variants that dominate strongly bound origins, which we denote as 'repetitive' and 'non-repetitive' (Figure 1D). Both variants contained a TTTAT stretch at the leading sub-motifl [5:10] but differed at the trailing sub-motif [11:16] location, which contained either a stretch of TTTxT, or a TTTAG sequence. Other origins included motif sequences that varied in the [5:10] and [11:16] positions, but those were fewer in count and weakly bound. Finally, Orc1 localized also to loci undergoing transcriptional silencing, where it has a role in the silencing process (25). Those included telomeric 'X elements', which contain the ORC motif, but also promoters of sub-telomeric and mating locus silenced genes lacking the motif, as determined by the absence of a sequence with a high motif score (methods) (Figure 1E, F). Below we examine the need of various ORC elements for binding these classes of sites.

A BAH domain explains Orc1 binding and activity at silenced loci

The function of Orc1 in gene silencing depends on its N-terminal BAH domain (44–51). This domain binds nucleosomes and interacts with silencing proteins (45,48). Early studies reported that this domain contributes to general ORC-chromatin association and is required for full binding in a subset of replication origins (52). Mapping the binding profile of Orc1 mutant lacking the BAH domain, we found that it was lost from silencing-associated sites, but remained bound to replication origins (Figure 2A, B). We also tested the binding of the 375-aa long Orc1 N-terminal tail containing the BAH domain (Figure 2C). While showing no binding at replication origins, this isolated element retained strong binding to all silencing-associated sites which was, again, BAH-dependent (Figure 2D, E). Therefore, the N-terminal tail is sufficient for Orc1 binding at silenced loci, but not in replication origins. Given the functional redundancy of silencing loci and its invariance to EACS deletion (53), described in the mating cassettes, these results suggest that Orc1 N-terminal tail is recruited to silencing loci through the BAH-mediated interaction with Sir1 (47). Further studies are needed to fully explore this relationship.

To examine whether the Orc1 N-terminal tail is sufficient for gene silencing itself, we quantified cell morphology changes associated with silencing. Specifically, cells of mating type 'a' harbor a mating type cassette whose silencing is required for cell elongation upon exposure to alpha factor ('shmooing'). Loss of silencing at the mating-type cassette abolishes this response and this was indeed reported for BAH-deleted cells (54). As predicted by the binding profile, the isolated Orc1 N-terminal tail was sufficient to rescue this silencing phenotype (Figure 2F). We conclude that our binding data is of sufficient resolution to capture the specific role of the BAH domain in Orc1 binding and activity at silencing-associated sites.

The Orc4 insertion helix is required for binding at non-repetitive but not repetitive motif sequence

The Orc4 insertion helix (Orc4-IH) was described in the cryo-EM structure as the only base-contacting ORC region in the DNA major groove. Subsequent studies raised the hypothesis that Orc4-IH determines motif specificity (23,24), and showed that Orc4-IH mutants exhibit slow growth, along with perturbed origin firing and replication-helicase loading (23,24).

We revisited the role of Orc4-IH by directly mapping the genomic binding of Orc4 mutated at two base-contacting residues (22) (substituting F485 and Y486 to Alanine; Figure 3A and Supplementary Figure S3). This mutant showed reduced binding at some origins (e.g. ARS1528, Figure 3B) but, perhaps unexpectedly, retained strong binding at others, including the origin used for structure determination (ARS305; Figure 3B). The binding effects were distinguished between the two ACS variants, with the non-repetitive motif exhibiting a much higher loss in binding (Figure 3C, D). This was also the case in telomeres, where motif-lacking silencing sites or repetitive motifs were not affected, while non-repetitive motif sites showed high loss of binding (Figure 3E). Note that Orc4-IH contacts nucleotides within the trailing T-stretch distinguishing the repetitive and non-repetitive motifs. We conclude that Orc4-IH expands ORC binding to sequences of reduced symmetry and T-content.

Orc1-BP4 is required for binding at replication origins, but is dispensable at silenced loci

The finding that Orc4-IH is required for binding at the non-repetitive, but not the repetitive motif sequence, motivated us to examine Orc1-BP4, the second base-interacting element seen in the cryo-EM structure. Previous studies using structural modeling (55,56) and conservation analysis (57) predicted a role for this BP in origin binding (Figure 4A), and mutating the *Drosophila* Orc1-BP reduced ORC-DNA affinity *in vitro* (43). Orc1-BP4 is essential for growth, which supports its general role in binding, but also complicates its analysis.

To overcome this, we mapped the binding of Orc1-BP4 mutants, while simultaneously introducing an exogenous (untagged) Orc1 copy. The wild type Orc1 copy maintained the viability, while the binding signal exclusively originated from ORC complexes incorporating the mutated copy, which was the only one fused to MNase (Supplementary Figure S4A). Verifying that this exogenous copy does not alter the measured binding profile of non-essential mutations (Figure 4B and Supplementary Figure S4B), we proceeded to analyze the binding of BP4-deleted Orc1. Deleting BP4 dramatically reduced Orc1 binding at most replication origins (Figure 4C), consistent with its insertion within the leading T-stretch (57)

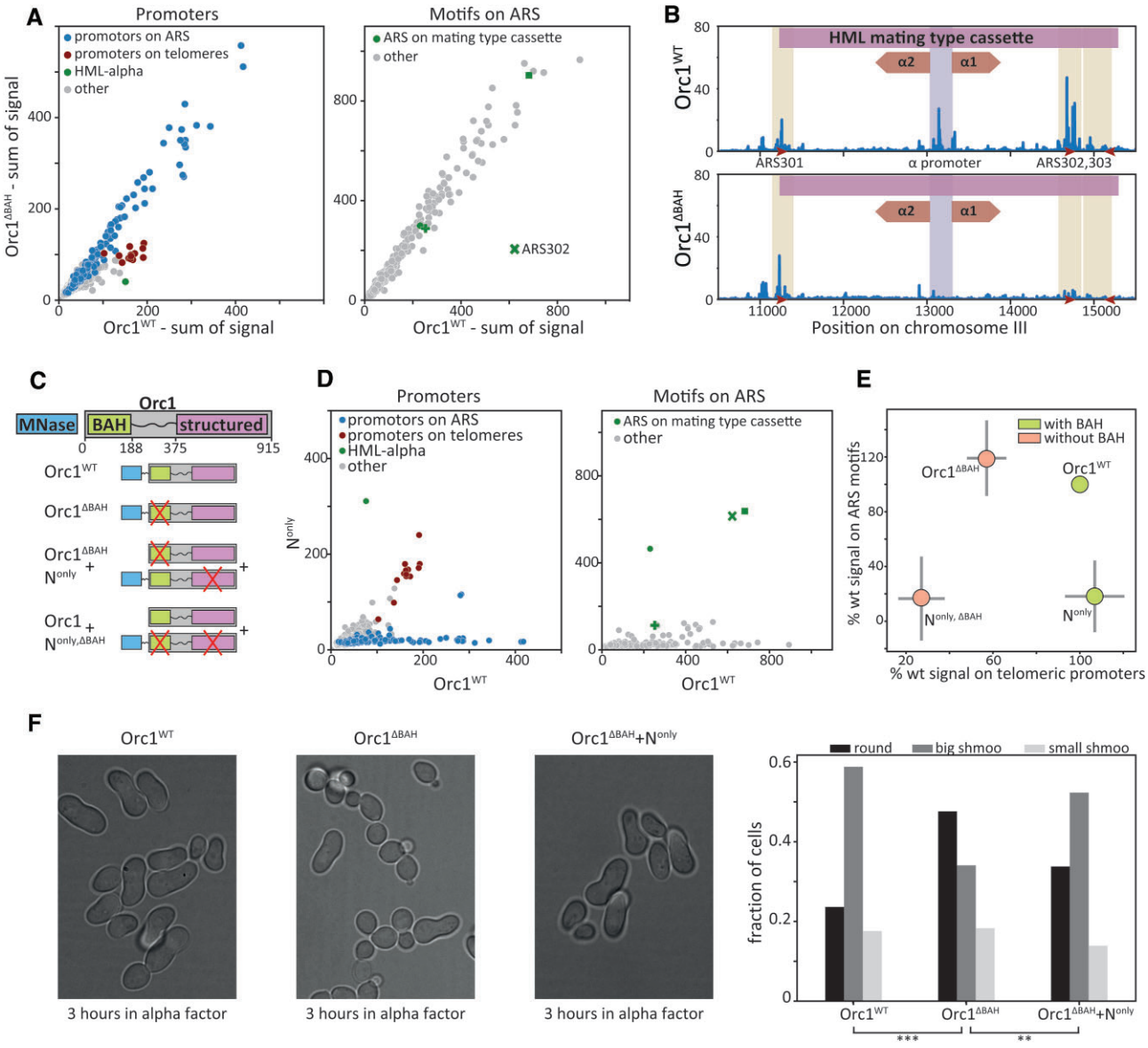

Figure 2. Orc1-BAH domain is necessary and sufficient for Orc1 binding and activity in silenced loci. (**A, B**) The Orc1 BAH domain is required for binding telomeric promoters but not replication origins: shown in A is the average binding on promoters (left) or replication origins (right), comparing the BAH-deleted Orc1 mutant (expressing only a mutated Orc1 from the endogenous locus) to the wild-type Orc1 strain. Each dot corresponds to one respective sequence, positioned by the overall number of reads assigned to this sequence. Read distribution over one segment – the mating type cassette - is also shown in (**B**). Here, ARS301 and ARS302/303 are inactive replication origins located at HML-E and HML-I silencers, respectively. A decrease in signal is primarily observed in the alpha genes promoter and in HML-I. Colors in (A) indicate promoters overlapping ARS elements (blue), promoters of telomere-located silenced genes (red), and promoter of silenced HML-alpha mating-type cassette (green). ARS sites on the mating type cassettes are colored green, with different shapes indicating their specific locations: HML-E (circle), HML-I (x), HMR-E (square) and HMR-I (+). Colors in (B) indicate mating factor alpha ORFs (red), promoter (gray) and origins (green), while ORC binding motifs are shown as red arrows. (C–E) Orc1 N-terminal tail binds to silenced loci in a BAH-dependent manner: we examined the binding of an isolated Orc1 N-terminal tail and several of its mutants, as illustrated schematically in (**C**). Shown are comparisons between the binding of the isolated Orc1-N terminal tail and the full Orc1 on promoters and origins (**D**, as in A above). The effects of the Orc1-N tail mutants are summarized in (**E**), showing the average change in binding (%) (with standard deviation in gray) over telomeric promoters lacking the ORC motif (x axis), and origins that do contain the motifs (y-axis). (See Supplementary Figure S2 for additional Orc1 N-terminal tail mutants). (**F**) The Orc1-N terminal tail rescues silencing phenotype of a strain deleted from the Orc1 BAH domain: A-type haploid cells of the indicated strains were incubated in alpha factor for 3 h and then visualized under the microscope. >600 cells were segmented and classified into three groups: round cells (insensitive to alpha factor), big shmoo (elongated, cell cycle arrested cells) and small shmoo (slightly elongated: ambiguous classification). (Left) examples of cells from each strain, (right) the fraction of cells of each type in the different strains.

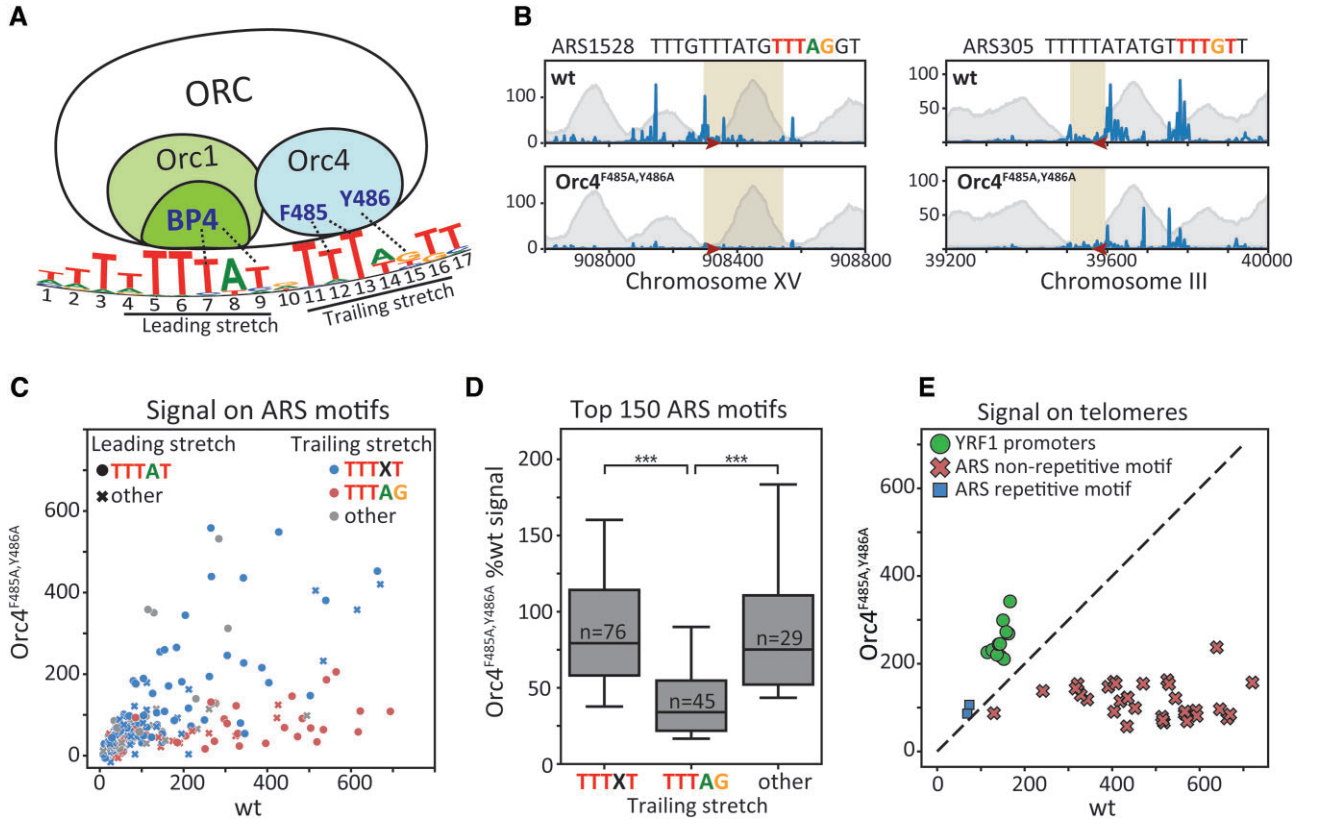

Figure 3. Orc4-IH stabilizes ORC binding specifically in replication origins containing a non-repetitive motif variant. (**A**) The two ORC components directly contact the EACS: a schematic representation based on the cryo-EM structure (22). (**B**) Orc4-IH is required for ORC binding at a subset of origins: shown is the Orc1 binding profiles at two representative replication origins (ARS1528 and ARS305), comparing binding of wild-type cells (wt) and cells carrying Orc4-IH mutation (Orc4-F485A,Y486A). Annotations as in Figure 1B above. (C, D) Orc4-IH mutation abolishes binding specifically at origins carrying the non-repetitive motif: a comparison of Orc1 binding signal across all origins is shown in (**C**), as measured in Orc4-F485A,Y486A mutant vs. wild-type cells. Each dot represents an origin, and its shape and color indicate the associated motif variant, as specified. Also shown (**D**) is the distribution of binding changes across origins containing the indicated motif variants. Asterisks denote *P*-values: $*P < 0.01$, $**P < 0.001$, $P***<0.0001$. (**E**) Orc1 retains strong binding at silenced loci in Orc4-IH mutant: Orc1 binding in the Orc4-F485A,Y486A mutant versus the wild-type cells on the indicated telomeric elements.

common to both motif sequences. Binding at silencing-associated sites was not affected (Supplementary Figure S4C).

Orc1-BP4 binding to DNA differs from the common paradigm of DNA-protein binding, as it involves the insertion of a disordered region within the minor groove (Figure 4D), providing little specificity. We were therefore interested in exploring the properties of this binding, and for this we used molecular dynamics (MD) simulations. We initiated the simulation with Orc1-BP4 being at the stable DNA-bound configuration, as described in the cryo-EM structure (22) (PDB ID: 5ZR1), and measured its subsequent confinement, as indicated by the standard deviation of the root mean square deviation (RMSD) across all the simulation steps. The intact BP4 showed little movement, as expected, but this confinement was lost when mutating either of the base-contacting residues to alanine (K362A and R367A), validating our simulations (Figure 4E). Testing eight additional mutants at different BP4 locations, we found that all retained DNA confinement. We conclude that local BP4-base interactions are sufficient to explain its DNA binding, while the surrounding residues are of smaller apparent effects.

We also tested these mutation effects experimentally by performing an alanine scan covering the 23 non-alanine residues within and surrounding Orc1-BP4 (Figure 4A). Contrasting our MD simulations, 17 out of 23 replacements did cause a substantial reduction in DNA binding (Figure 4F). Effects were correlated across mutants (Figure 4G) with PCA analysis attributing 88% of the variation to a single component (Supplementary Figure S4D), and were well explained by the distance to the two base-contacting residues (K362, R367) or their minor-groove embedded assisting residues (F360, Y372) (Figure 4D). While failure of the mutated Orc1 to integrate into the complex could be the cause for the reduced signal, we find it improbable given the cryo-EM structure. This region is embedded in the DNA, rather than being part of the domains responsible for complex formation. Also, most mutants were viable without the wild-type copy, indicating successful integration and the remaining five lethal mutations were in residues deeply embedded in the DNA. We also measured growth phenotypes of those same mutants, using strains that lacked the endogenous copy, and those correlated well with the loss of binding ($R^2 = 0.90$, P value $= 7.5 \times 10^{-9}$), including the apparent essentiality (inability to generate) of the five mutants showing strongest binding effects (K362A, R367A, F360A, Y372A, K359A) (Figure 4F, H). Therefore, the *in vivo* Orc1-BP4-DNA binding depends on multiple BP4 residues, surrounding the base-contacting ones.

The partial agreement between the MD simulations and the measured phenotypes of BP4 mutants suggests that additional factors, not included in the simulations, influence BP4-DNA

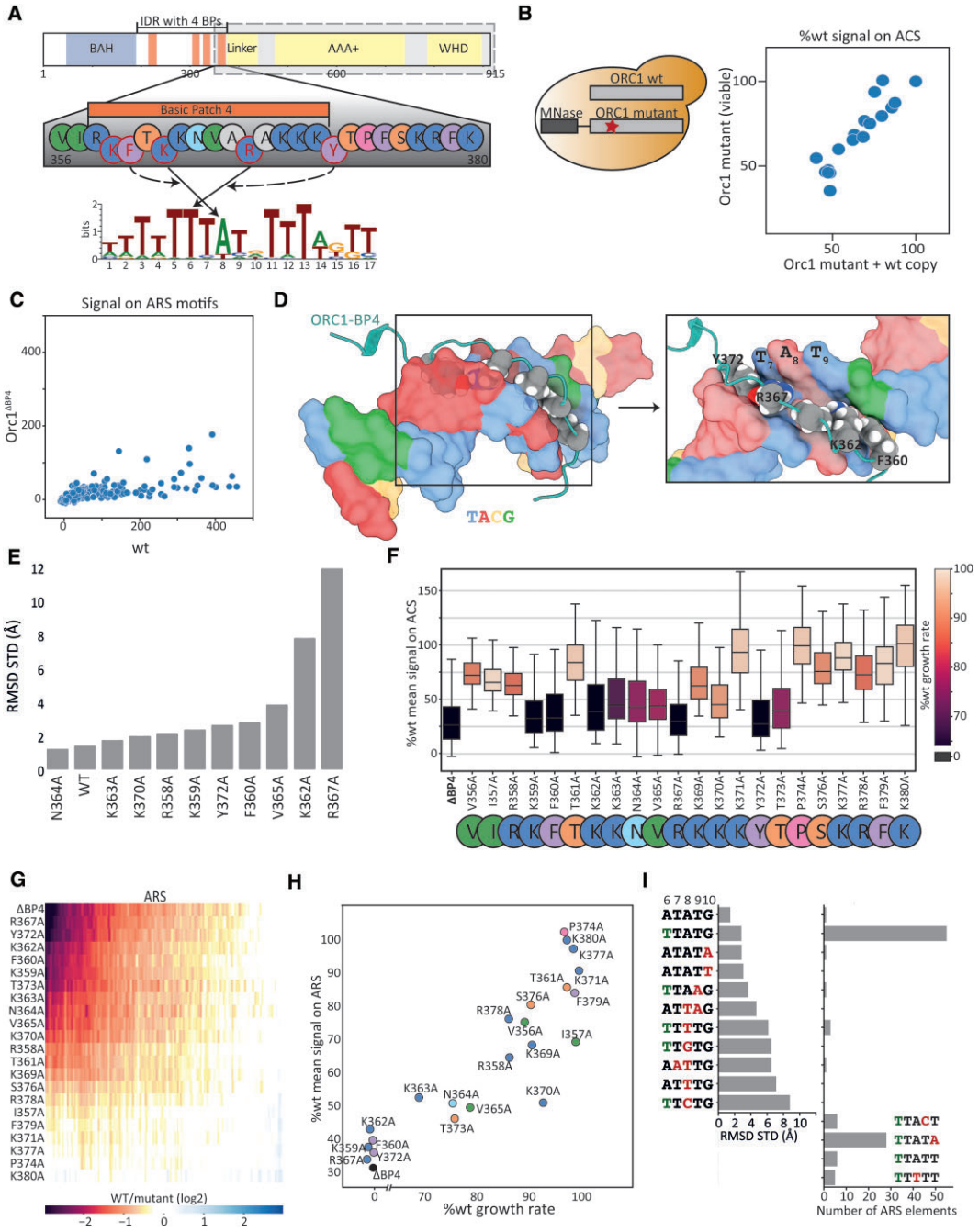

Figure 4. Orc1-BP4 stabilizes binding at all replication origins, depending on multiple residues beside the direct base-contacting ones. (**A**) Orc1-BP4 interaction with the ORC motif: a scheme based on the cryo-EM structure (22). Full and dashed arrows indicate specific DNA-base contacts and predicted 'supportive' residues, respectively. (**B**) Binding profile of lethal mutations is measured by adding an exogenous wild-type allele: deleting Orc1-BP4 or mutating its residues often resulted in a lethal or slow-growth phenotype (see below). To still map their binding, we engineered a strain containing an intact Orc1 copy and a mutant Orc1 fused to MNase, as illustrated (left). This enabled mapping of the mutant allele (further explanation in Supplementary Figure S4A), as we verified by profiling viable mutants in the presence or absence of the wild-type copy and subsequently comparing them. Shown here are the median binding signal across origins in the presence or absence of the additional wild-type Orc1 copy (right) (see Supplementary Figure S4B for specific mutation comparisons). (**C**). Orc1-BP4 deletion abolishes Orc1 binding at all origins: shown is the binding signal of Orc1 lacking BP4 (y-axis) compared to intact Orc1 (x-axis) across all replication origins. (**D**) Atomic view of Orc1-BP4 (cyan) inserted into the DNA minor groove, as described by the cryo-EM model (22): direct binding amino acids located in the minor groove are labeled, and each nucleotide is color-coded: T in blue, A in red, C in orange, and G in green. (**E**) MD simulations predictions of Orc1-BP4 mutant effects: shown is the predicted conformational stability of the indicated BP4 mutants. Conformational stability was estimated by the plasticity of Orc1-BP4 localization at its binding site, as quantified by the standard deviation of the root mean square deviation (over all the simulation steps) relative to the localization seen in the cryo-EM structure (PDB ID 5ZR1). (F–H) Multiple BP4 residues beyond the base-contacting ones contribute to motif binding: shown in (**F**) are the distributions of binding signals of the indicated Orc1-BP4 mutants, relative to the wild-type Orc1-BP4, across all origins. Colors indicate mutant growth rates. Also shown are the fold-change in binding relative to wild-type BP4 across individual origins (**G**), and a direct comparison of the average change in binding and mutant growth rate (**H**). (**I**) MD simulations do not explain the conservation of the Orc1 binding motif: shown on the left are conformational heterogeneities observed when simulating binding of intact Orc1-BP4 to the indicated motif variants. Mutations are marked in red, while T6 of the conserved motif is denoted in green. Results are compared to the number of occurrences of the specified variants among the 150 top-bound origins in the genome (right).

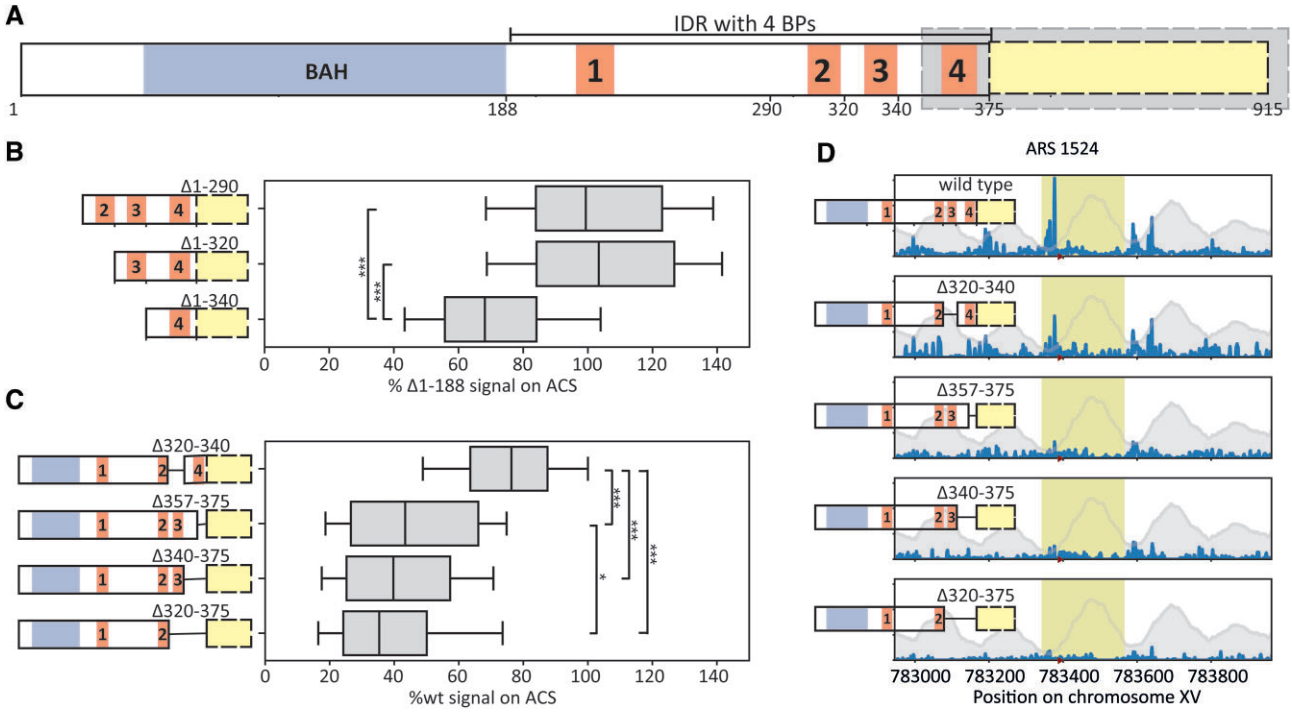

Figure 5. ORC1-BP3 contributes to origin binding. (**A**) Schematic representation of Orc1 N-terminal tail: colors as in Figure 1A. Note the four basic patches (BPs) within the intrinsically disordered region (IDR). The cryo-EM structure (22) was solved using a truncated Orc1, containing the 355–914 AA (gray). (B–D) Orc1-BP3 deletions reduces origin binding: shown in (**B, C**) are the distributions of origin binding of the indicated mutants. Data are shown relative to the 188aa-truncated strain (BAH deletion, B) or intact Orc1 (C). The respective reads distribution across a selected origin is also shown (**D**).

binding *in vivo*. BP4, for example, could interact with other ORC components, and we noted some indications for this within the structure (Supplementary Figure S4E). Perturbation of such intramolecular interactions within ORC1 may affect its DNA-binding affinity. Alternatively, some mutations might affect transient BP4 interactions with nonspecific DNA sites that are required for guiding Orc1 to its high-affinity binding at the specific site. Such mutations may affect the overall binding preferences of ORC1 along genomic DNA but would be invisible to our MD simulations or the structure. In this latter case, MD predictions would also be blind to mutating DNA bases participating in those transient interactions because quantifying their effect demands dynamics and kinetic characterization (58), which is not accessible to the atomistic modeling.

To test this, we simulated BP4 interaction with different mutated DNA sequences (Figure 4I). First, we noted that the motif sequence used in the structure (PDB ID: 5ZR1), and therefore our simulations, differed from the canonical one, although it was still strongly bound *in vivo*. Mutating this sequence to retrieve the canonical abundant ACS retained strong binding, while mutating the conserved A base at the center of BP4-DNA interactions (position 8 in the motif) abrogated BP4 confinement, validating our simulations. Notably, mutating other conserved residues 2bp apart from the core interactions, had no or little effect on confinement within our simulations, although the respective DNA sequences were lacking, or weakly bound *in vivo* (Figure 4I). Taken together, these results suggest that transient BP4 interactions with semi-specific DNA sites guide ORC to its high-affinity binding, but these are invisible in both the MD simulations and structural analysis, which report on the local binding stability.

BP3 is essential for ORC binding in the absence of Orc4-IH interacting residues

Our results so far have revealed that binding at the non-repetitive EACS requires both Orc1-BP4 and Orc4-IH, while binding the repetitive motif requires only Orc1-BP4. This raised the question of whether the latter binding depends on an additional ORC element. Since Orc1-BP4 and Orc4-IH were the only base-contacting elements seen in the structure, we next considered the Orc1 N-terminal tail that was absent from the Orc1 used for the structure analysis (22) (Figure 5A). This tail borders BP4 and includes three additional basic patches. We found that truncating the proximal two had no detectable effect on ARS binding, but a longer truncation that included BP3 reduced ORC binding (Figure 5B). We further profiled four additional Orc1 mutants: one that lacked only BP3 (residues 320–340), two that lacked BP4 (residues 357–375 or residues 340–375), and a mutant that lacked both BP3 and BP4 (residues 320–375). Consistently, deleting BP3 alone led to a moderate reduction in binding, while co-deletion of BP3 and BP4 accentuated the effect of BP4 deletion (Figure 5C, D).

As expected, Orc1-BP3 deletion affected the repetitive EACS (Figure 6A, B). We therefore hypothesized that ORC1-BP3 and ORC4-IH play a complementary role in stabilizing ORC and examined this by combining the Orc1-BP3 and Orc4-IH mutations (Orc4 F485A and Y486A). Indeed, while the individual mutants were viable, we could not generate the combination, suggesting lethality. To verify this interaction at the level of ORC binding, we introduced the Orc4-IH mutations into cells carrying a deleted Orc1-BP3 tagged with MNase, as well as an intact (unlabeled) Orc1 (as illustrated in Figure 4B). As predicted, BP3 was essential for ORC bind-

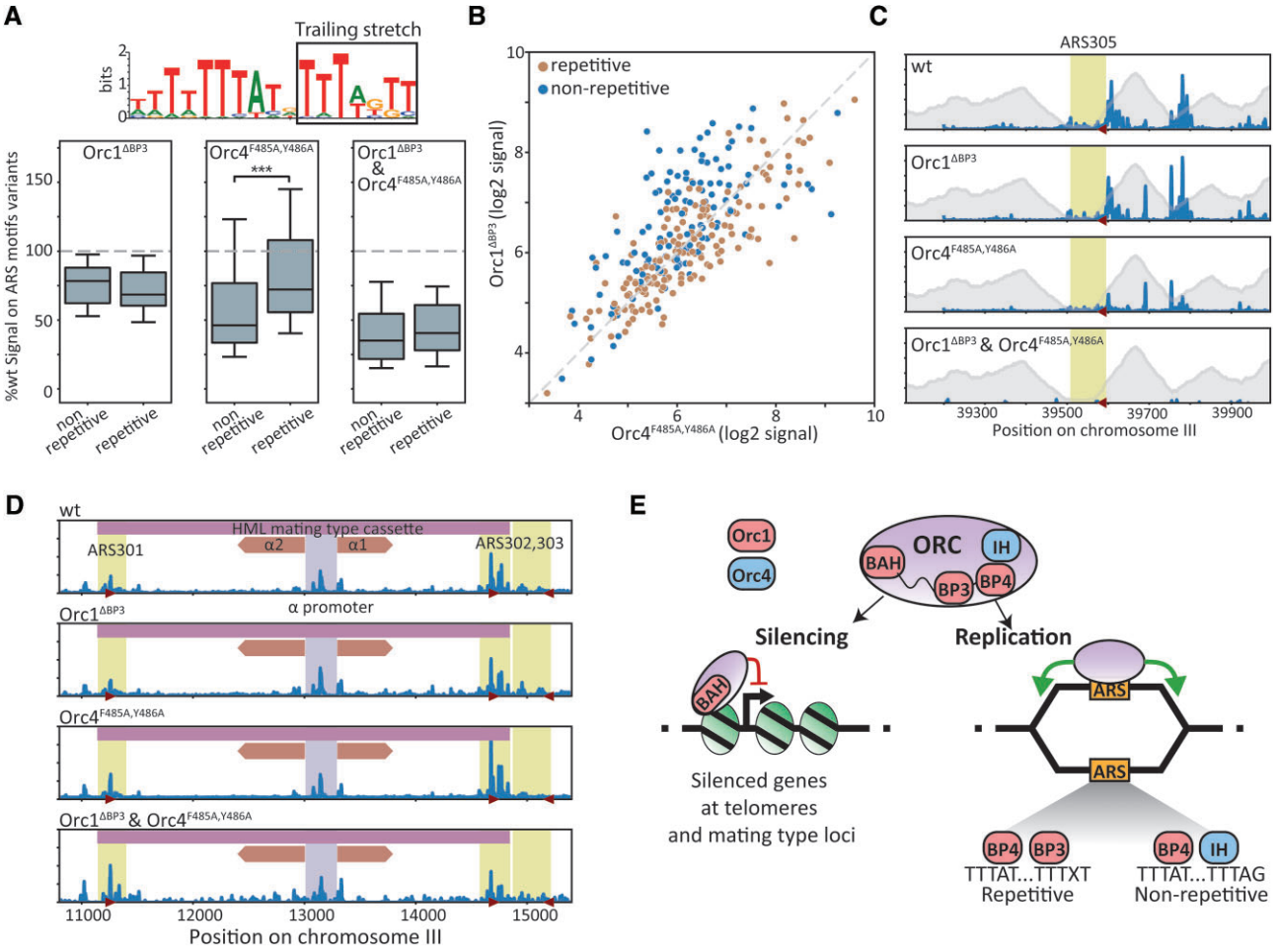

Figure 6. Orc1-BP3 and Orc4-IH play complementary roles in stabilizing ORC binding at replication origins. (A–C) Orc1-BP3 is essential for origin binding in Orc4-IH mutant cells: shown in (**A**) are the distributions of origin binding in the indicated single and double mutants. Origins containing the repetitive or non-repetitive motifs variants are shown separately. Also shown are the effects of the individual mutants on individual origins, with colors indicating the associated motif variant (**B**), and the reads aligned to the origin in the cryo-EM structure (22) (**C**, annotation as in Figure 1B). (**D**) Distributions of binding of the indicated mutants to the silenced HML mating type cassette. (**E**) A model – three distinct modes of ORC-DNA binding: in promoters of silenced genes lacking the motif, the Orc1-BAH domain is necessary and sufficient for binding. In replication origins, ORC binding differs depending on the motif variants. Orc1-BP4 is required for both sets, but an additional anchor is required to stabilize binding, and this is provided by either Orc4-IH or Orc1-BP3, with the latter able to only supplement Orc4-IH at the repetitive motif variant.

ing at replication origins when Orc4-IH was mutated (Figure 6A, C), with binding remaining only at silencing-associated loci (Figure 6D). We conclude that Orc1-BP3 and Orc4-IH can both complement Orc1-BP4 in stabilizing ORC binding. In this, Orc4-IH is required for the non-repetitive EACS, while Orc1-BP3 can bind the repetitive one.

Discussion

The ORC lacks an apparent DNA binding domain but still localizes specifically to certain DNA sequences, which, in budding yeast, are marked by a 17-bp T-rich motif. Structural analysis partially explained this preference by revealing two ORC elements that directly contact five motif bases. One of these (Orc4-IH) inserts within the major groove, while the second (Orc1-BP4) inserts into the minor groove, providing little base discrimination. Those limited interactions raised the question of whether they are sufficient to explain ORC-DNA binding *in vivo*, and motivated our study.

We improved the spatial resolution of ORC binding locations using ChEC-seq, which revealed previously unrecognized classes of ORC binding motifs: a repetitive sequence that contained two T-stretches (a leading TTTAT and a trailing TTTxT) and a non-repetitive class that contained the same leading stretch, but a trailing TTTAG stretch. Further analysis revealed that ORC binding differs between those variants. Orc1-BP4 was required for binding at both, consistent with its insertion at the common leading stretch, while Orc4-IH was only needed for binding to the non-repetitive motif. At the repetitive motif, Orc4-IH was not required, and could be compensated by a second basic-patch, Orc1-BP3, that was absent from the structure.

To gain further insights into ORC-DNA binding, we delved deeper into Orc1-BP4 interactions through mutation analysis, combining MD simulations and experiments. It is notable that our simulations reproduced well the phenotypes of the direct contact sites, on both DNA and the peptides. However, they were blind to the effects of additional Orc1 residues or DNA elements positioned a few residues apart. These differences could result from additional interactions not included in our simulations. Yet, their prevalence on both DNA and BP4 itself leads us to favor an alternative explanation, in which ORC-DNA binding depends on transient BP4-motif interac-

tions. Although transient only, these interactions can still dominate the mechanism and speed for reaching the high-affinity site visible to the structure and MD simulations. Modulating the rate of binding to the DNA motif can directly affect the efficiency of high-affinity binding, and therefore functionality (59).

Based on this, and the revealed symmetry of both the motif and the associated Orc1-BP interactors, we propose a model (Figure 6E) in which BPs within the Orc1-N terminal tail favor sliding within the minor grooves of T-stretches. This sliding is stabilized when reaching a non-T residue, as in TTTxT. We further propose that two such interactions are required, as individual ones are not strong enough. In motifs that lack the second TTTxT stretch, this role is overtaken by Orc4-IH which interacts with an alternative TTTAG sequence. Further studies are required to test this model.

The *S. cerevisiae* ORC used in this study is unique in preferring a specific sequence motif. Other eukaryotic ORCs do not show this preference, but still localize to specific T-rich genomic locations. Based on the conservation of BPs within the Orc1 N-terminus, we propose that ORC-DNA binding is guided by those BPs through a conserved mechanism common also to *S. cerevisiae*, potentially with slight alterations tuned for the requirements of each genome, as exemplified by Orc4-IH in budding yeast.

Data availability

The raw sequencing reads and processed coverage profiles are accessible on GEO (GSE249817).

The code for analyzing the data and generating the figures is available at https://doi.org/10.5281/zenodo.10305064.

Supplementary data

Supplementary Data are available at NAR Online.

Acknowledgements

We thank Joseph Steinberger for his guidance and assistance in conducting the microscopy experiments. We thank Gilad Yaakov, Sagie Brodsky, Felix Jonas and Alon Chappleboim for their insightful comments and suggestions on the manuscript. Special thanks are also due to the entire Barkai lab for creating a stimulating atmosphere and engaging in fruitful discussions.

Funding

European Research Council (ERC); Israel Science Foundation (ISF); Minerva. Funding for open access charge: Weizmann Institute of Science, Department of Molecular Genetics.

Conflict of interest statement

None declared.

References

1. Leonard,A.C. and Méchali,M. (2013) DNA replication origins. *Cold Spring Harb. Perspect. Biol.*, **5**, a010116.
2. Punjani,A., Rubinstein,J.L., Fleet,D.J. and Brubaker,M.A. (2017) cryoSPARC: algorithms for rapid unsupervised cryo-EM structure determination. *Nat. Methods*, **14**, 290–296.
3. Bell,S.P. and Labib,K. (2016) Chromosome duplication in saccharomyces cerevisiae. *Genetics*, **203**, 1027–1067.
4. Bleichert,F., Balasov,M., Chesnokov,I., Nogales,E., Botchan,M.R. and Berger,J.M. (2013) A Meier-Gorlin syndrome mutation in a conserved C-terminal helix of Orc6 impedes origin recognition complex formation. *eLife*, **2**, e00882.
5. On,K.F., Jaremko,M., Stillman,B. and Joshua-Tor,L. (2018) A structural view of the initiators for chromosome replication. *Curr. Opin. Struct. Biol.*, **53**, 131–139.
6. Kawakami,H. and Katayama,T. (2010) DnaA, ORC, and Cdc6: similarity beyond the domains of life and diversity. *Biochem. Cell Biol.*, **88**, 49–62.
7. Rao,H. and Stillman,B. (1995) The origin recognition complex interacts with a bipartite DNA binding site within yeast replicators. *Proc. Natl. Acad. Sci. U.S.A.*, **92**, 2224–2228.
8. Marahrens,Y. and Stillman,B. (1992) A yeast chromosomal origin of DNA replication defined by multiple functional elements. *Science*, **255**, 817–823.
9. Newlon,C.S. and Theis,J.F. (1993) The structure and function of yeast ARS elements. *Curr. Opin. Genet. Dev.*, **3**, 752–758.
10. Newlon,C.S. and Theis,J.F. (2002) DNA replication joins the revolution: whole-genome views of DNA replication in budding yeast. *Bioessays*, **24**, 300–304.
11. Wilmes,G.M. and Bell,S.P. (2002) The B2 element of the Saccharomyces cerevisiae ARS1 origin of replication requires specific sequences to facilitate pre-RC formation. *Proc. Natl. Acad. Sci. U.S.A.*, **99**, 101–106.
12. Theis,J.F. and Newlon,C.S. (1994) Domain B of ARS307 contains two functional elements and contributes to chromosomal replication origin function. *Mol. Cell. Biol.*, **14**, 7652–7659.
13. Theis,J.F., Yang,C., Schaefer,C.B. and Newlon,C.S. (1999) DNA sequence and functional analysis of homologous ARS elements of saccharomyces cerevisiae and S. carlsbergensis. *Genetics*, **152**, 943–952.
14. Theis,J.F. and Newlon,C.S. (1997) The ARS309 chromosomal replicator of Saccharomyces cerevisiae depends on an exceptional ARS consensus sequence. *Proc. Natl. Acad. Sci. U.S.A.*, **94**, 10786–10791.
15. Eaton,M.L., Galani,K., Kang,S., Bell,S.P. and MacAlpine,D.M. (2010) Conserved nucleosome positioning defines replication origins. *Genes Dev.*, **24**, 748–753.
16. Xu,W., Aparicio,J.G., Aparicio,O.M. and Tavaré,S. (2006) Genome-wide mapping of ORC and Mcm2p binding sites on tiling arrays and identification of essential ARS consensus sequences in S. cerevisiae. *Bmc Genomics [Electronic Resource]*, **7**, 276.
17. Austin,R.J., Orr-Weaver,T.L. and Bell,S.P. (1999) Drosophila ORC specifically binds to ACE3, an origin of DNA replication control element. *Genes Dev.*, **13**, 2639–2649.
18. Chesnokov,I., Remus,D. and Botchan,M. (2001) Functional analysis of mutant and wild-type Drosophila origin recognition complex. *Proc. Natl. Acad. Sci. U.S.A.*, **98**, 11997–12002.
19. Kong,D., Coleman,T.R. and DePamphilis,M.L. (2003) Xenopus origin recognition complex (ORC) initiates DNA replication preferentially at sequences targeted by Schizosaccharomyces pombe ORC. *EMBO J.*, **22**, 3441–3450.
20. Vashee,S., Cvetic,C., Lu,W., Simancek,P., Kelly,T.J. and Walter,J.C. (2003) Sequence-independent DNA binding and replication initiation by the human origin recognition complex. *Genes Dev.*, **17**, 1894–1908.
21. Liu,J., Zimmer,K., Rusch,D.B., Paranjape,N., Podicheti,R., Tang,H. and Calvi,B.R. (2015) DNA sequence templates adjacent nucleosome and ORC sites at gene amplification origins in Drosophila. *Nucleic Acids Res.*, **43**, 8746–8761.
22. Li,N., Lam,W.H., Zhai,Y., Cheng,J., Cheng,E., Zhao,Y., Gao,N. and Tye,B.-K. (2018) Structure of the origin recognition complex bound to DNA replication origin. *Nature*, **559**, 217–222.
23. Lee,C.S.K., Cheung,M.F., Li,J., Zhao,Y., Lam,W.H., Ho,V., Rohs,R., Zhai,Y., Leung,D. and Tye,B.-K. (2021) Humanizing the yeast origin recognition complex. *Nat. Commun.*, **12**, 33.
24. Hu,Y., Tareen,A., Sheu,Y.-J., Ireland,W.T., Speck,C., Li,H., Joshua-Tor,L., Kinney,J.B. and Stillman,B. (2020) Evolution of DNA replication origin specification and gene silencing mechanisms. *Nat. Commun.*, **11**, 5175.

25. Fox,C.A. and McConnell,K.H. (2005) Toward biochemical understanding of a transcriptionally silenced chromosomal domain in Saccharomyces cerevisiae. *J. Biol. Chem.*, **280**, 8629–8632.
26. Cong,L., Ran,F.A., Cox,D., Lin,S., Barretto,R., Habib,N., Hsu,P.D., Wu,X., Jiang,W., Marraffini,L.A., *et al.* (2013) Multiplex genome engineering using CRISPR/Cas systems. *Science*, **339**, 819–823.
27. Anand,R., Memisoglu,G. and Haber,J. (2017) Cas9-mediated gene editing in *Saccharomyces cerevisiae*. *Protocol Exchange*, https://doi.org/10.1038/protex.2017.021a.
28. Gietz,R.D., Schiestl,R.H., Willems,A.R. and Woods,R.A. (1995) Studies on the transformation of intact yeast cells by the LiAc/SS-DNA/PEG procedure. *Yeast*, **11**, 355–360.
29. Zentner,G.E., Kasinathan,S., Xin,B., Rohs,R. and Henikoff,S. (2015) ChEC-seq kinetics discriminates transcription factor binding sites by DNA sequence and shape in vivo. *Nat. Commun.*, **6**, 8733.
30. Skene,P.J. and Henikoff,S. (2017) An efficient targeted nuclease strategy for high-resolution mapping of DNA binding sites. *eLife*, **6**, e21856.
31. Blecher-Gonen,R., Barnett-Itzhaki,Z., Jaitin,D., Amann-Zalcenstein,D., Lara-Astiaso,D. and Amit,I. (2013) High-throughput chromatin immunoprecipitation for genome-wide mapping of in vivo protein-DNA interactions and epigenomic states. *Nat. Protoc.*, **8**, 539–554.
32. Martin,M. (2011) Cutadapt removes adapter sequences from high-throughput sequencing reads. *EMBnet.journal*, **17**, 10–12.
33. Langmead,B. and Salzberg,S.L. (2012) Fast gapped-read alignment with Bowtie 2. *Nat. Methods*, **9**, 357–359.
34. Cherry,J.M., Hong,E.L., Amundsen,C., Balakrishnan,R., Binkley,G., Chan,E.T., Christie,K.R., Costanzo,M.C., Dwight,S.S., Engel,S.R., *et al.* (2012) Saccharomyces Genome Database: the genomics resource of budding yeast. *Nucleic Acids Res.*, **40**, D700–D705.
35. de Boer,C.G. and Hughes,T.R. (2012) YeTFaSCo: a database of evaluated yeast transcription factor sequence specificities. *Nucleic Acids Res.*, **40**, D169–D179.
36. Lu,A.X., Zarin,T., Hsu,I.S. and Moses,A.M. (2019) YeastSpotter: accurate and parameter-free web segmentation for microscopy images of yeast cells. *Bioinformatics*, **35**, 4525–4527.
37. Pronk,S., Páll,S., Schulz,R., Larsson,P., Bjelkmar,P., Apostolov,R., Shirts,M.R., Smith,J.C., Kasson,P.M., van der Spoel,D., *et al.* (2013) GROMACS 4.5: a high-throughput and highly parallel open source molecular simulation toolkit. *Bioinformatics*, **29**, 845–854.
38. Belsky,J.A., MacAlpine,H.K., Lubelsky,Y., Hartemink,A.J. and MacAlpine,D.M. (2015) Genome-wide chromatin footprinting reveals changes in replication origin architecture induced by pre-RC assembly. *Genes Dev.*, **29**, 212–224.
39. Diffley,J.F. and Cocker,J.H. (1992) Protein-DNA interactions at a yeast replication origin. *Nature*, **357**, 169–172.
40. Cocker,J.H., Piatti,S., Santocanale,C., Nasmyth,K. and Diffley,J.F. (1996) An essential role for the Cdc6 protein in forming the pre-replicative complexes of budding yeast. *Nature*, **379**, 180–182.
41. Speck,C., Chen,Z., Li,H. and Stillman,B. (2005) ATPase-dependent cooperative binding of ORC and Cdc6 to origin DNA. *Nat. Struct. Mol. Biol.*, **12**, 965–971.
42. Bell,S.P. and Stillman,B. (1992) ATP-dependent recognition of eukaryotic origins of DNA replication by a multiprotein complex. *Nature*, **357**, 128–134.
43. Bleichert,F., Leitner,A., Aebersold,R., Botchan,M.R. and Berger,J.M. (2018) Conformational control and DNA-binding mechanism of the metazoan origin recognition complex. *Proc. Natl. Acad. Sci. U.S.A.*, **115**, E5906–E5915.
44. Brand,A.H., Micklem,G. and Nasmyth,K. (1987) A yeast silencer contains sequences that can promote autonomous plasmid replication and transcriptional activation. *Cell*, **51**, 709–719.
45. Gasser,S.M. and Cockell,M.M. (2001) The molecular biology of the SIR proteins. *Gene*, **279**, 1–16.
46. Grunstein,M. and Gasser,S.M. (2013) Epigenetics in Saccharomyces cerevisiae. *Cold Spring Harb. Perspect. Biol.*, **5**, a017491.
47. Hou,Z., Bernstein,D.A., Fox,C.A. and Keck,J.L. (2005) Structural basis of the Sir1–origin recognition complex interaction in transcriptional silencing. *Proc. Natl. Acad. Sci. U.S.A.*, **102**, 8489–8494.
48. Kueng,S., Oppikofer,M. and Gasser,S.M. (2013) SIR proteins and the assembly of silent chromatin in budding yeast. *Annu. Rev. Genet.*, **47**, 275–306.
49. Martino,F., Kueng,S., Robinson,P., Tsai-Pflugfelder,M., van Leeuwen,F., Ziegler,M., Cubizolles,F., Cockell,M.M., Rhodes,D. and Gasser,S.M. (2009) Reconstitution of yeast silent chromatin: multiple contact sites and O-AADPR binding load SIR complexes onto nucleosomes in vitro. *Mol. Cell*, **33**, 323–334.
50. Triolo,T. and Sternglanz,R. (1996) Role of interactions between the origin recognition complex and SIR1 in transcriptional silencing. *Nature*, **381**, 251–253.
51. Geissenhöner,A., Weise,C. and Ehrenhofer-Murray,A.E. (2004) Dependence of ORC silencing function on NatA-mediated nalpha acetylation in saccharomyces cerevisiae. *Mol. Cell. Biol.*, **24**, 10300–10312.
52. Müller,P., Park,S., Shor,E., Huebert,D.J., Warren,C.L., Ansari,A.Z., Weinreich,M., Eaton,M.L., MacAlpine,D.M. and Fox,C.A. (2010) The conserved bromo-adjacent homology domain of yeast Orc1 functions in the selection of DNA replication origins within chromatin. *Genes Dev.*, **24**, 1418–1433.
53. McNally,F.J. and Rine,J. (1991) A synthetic silencer mediates SIR-dependent functions in Saccharomyces cerevisiae. *Mol. Cell. Biol.*, **11**, 5648–5659.
54. Zhang,Z., Hayashi,M.K., Merkel,O., Stillman,B. and Xu,R.-M. (2002) Structure and function of the BAH-containing domain of Orc1p in epigenetic silencing. *EMBO J.*, **21**, 4600–4611.
55. Sun,J., Kawakami,H., Zech,J., Speck,C., Stillman,B. and Li,H. (2012) Cdc6-induced conformational changes in ORC bound to origin DNA revealed by cryo-electron microscopy. *Structure*, **20**, 534–544.
56. Sun,J., Evrin,C., Samel,S.A., Fernández-Cid,A., Riera,A., Kawakami,H., Stillman,B., Speck,C. and Li,H. (2013) Cryo-EM structure of a helicase loading intermediate containing ORC-Cdc6-Cdt1-MCM2-7 bound to DNA. *Nat. Struct. Mol. Biol.*, **20**, 944–951.
57. Kawakami,H., Ohashi,E., Kanamoto,S., Tsurimoto,T. and Katayama,T. (2015) Specific binding of eukaryotic ORC to DNA replication origins depends on highly conserved basic residues. *Sci. Rep.*, **5**, 14929.
58. Bigman,L.S. and Levy,Y. (2023) Protein diffusion along Protein and DNA lattices: role of electrostatics and disordered regions. *Annu. Rev. Biophys.*, **52**, 463–486.
59. Zandarashvili,L., Esadze,A., Vuzman,D., Kemme,C.A., Levy,Y. and Iwahara,J. (2015) Balancing between affinity and speed in target DNA search by zinc-finger proteins via modulation of dynamic conformational ensemble. *Proc. Natl. Acad. Sci. U.S.A.*, **112**, E5142–E9.
60. Dosztányi,Z., Csizmók,V., Tompa,P. and Simon,I. (2005) The pairwise energy content estimated from amino acid composition discriminates between folded and intrinsically unstructured proteins. *J. Mol. Biol.*, **347**, 827–839.
61. Dosztányi,Z., Csizmok,V., Tompa,P. and Simon,I. (2005) IUPred: web server for the prediction of intrinsically unstructured regions of proteins based on estimated energy content. *Bioinformatics*, **21**, 3433–3434.
62. Chapal,M., Mintzer,S., Brodsky,S., Carmi,M. and Barkai,N. (2019) Resolving noise–control conflict by gene duplication. *PLoS Biol.*, **17**, e3000289.
63. Yabuki,N., Terashima,H. and Kitada,K. (2002) Mapping of early firing origins on a replication profile of budding yeast. *Genes Cells*, **7**, 781–789.

Received: January 10, 2024. **Revised:** March 16, 2024. **Editorial Decision:** March 23, 2024. **Accepted:** April 9, 2024